A SPARSE SPECTRAL DECONVOLUTION ALGORITHM FOR NON-CARTESIAN MRSI

Sampada Bhave[1] *, Ramin Eslami*[2] *, Mathews Jacob*[1]

[1] *Department of Electrical and Computer Engineering, University of Iowa , Iowa*

[2] *Media Processing Technology Lab, Sony Electronics, San Jose, CA 95112*

Correspondence to :

Mathews Jacob,

Department of Electrical and Computer Engineering,

Iowa City, IA 52242

email: Mathews-Jacob@uiowa.edu

phone number: 319-335-6420.

Manuscript word count: abstract (183),body (2782)

Running title: MRSI reconstruction using spectral deconvolution

Abstract

Purpose: To minimize line shape distortions and spectral leakage artifacts in MR spectroscopic imaging.

Methods: A spatially and spectrally regularized non-Cartesian MRSI algorithm that uses the line shape distortion priors, estimated from water reference data, to deconvolve the spectra is introduced. Sparse spectral regularization is used to minimize noise amplification associated with deconvolution. A spiral MRSI sequence, that heavily oversamples the central k-space regions is used to acquire the MRSI data. The spatial regularization term uses the spatial supports of brain and extra-cranial fat regions to recover the metabolite spectra and nuisance signals at two different resolutions. Specifically, the nuisance signals are recovered at the maximum resolution to minimize spectral leakage, while the point spread functions of metabolites are controlled to obtain acceptable signal to noise ratio.

Results: The comparisons of the algorithm against Tikhonov regularized reconstructions demonstrates considerably reduced line shape distortions and improved metabolite maps.

Conclusion: The proposed sparsity constrained spectral deconvolution scheme is effective in minimizing the line shape distortions. The dual resolution reconstruction scheme is capable of minimizing spectral leakage artifacts.

1 INTRODUCTION

The spatial resolution at which robust MR spectroscopic imaging (MRSI) data can be acquired in a clinically feasible scan time is considerably lower than other MRI methods, inspite of fast scan MRSI sequences (1–6). Specifically, the low concentration of the metabolites introduces a strict tradeoff between achievable spatial resolution and signal to noise ratio (SNR). The large voxel sizes often causes several artifacts including magnetic field inhomogeneity induced line shape distortions and spectral leakage from extra-cranial lipids and unsuppressed water. Model based algorithms were introduced to overcome these problems by extrapolating the k-space data using high resolution brain segmentations (e.g. to gray matter, white matter, and cerebral spinal fluid regions) (7–10). The clinical utility of these schemes are restricted due to risk of biased reconstructions.

Variable density spiral MRSI schemes are reported to provide a better compromise between SNR and k-space coverage than Cartesian trajectories because they oversample k-space center (3, 11). Current non-Cartesian reconstruction methods independently recover each temporal frame of the spatio-temporal data using 2-D image reconstruction algorithms (3–5, 11). While this approach is computationally efficient, this strategy makes it difficult to exploit spatial-spectral correlations in the data and to compensate for line shape distortions. In addition, current non-Cartesian algorithms are designed to recover the entire image with the same resolution; the direct use of these methods in MRSI often results in undesirable tradeoffs. Specifically, recovering the dataset at a low resolution will result in spectral leakage from nuisance signals, while high resolution recovery will yield poor signal to noise ratio (SNR).

We propose a novel iterative non-Cartesian MRSI algorithm to jointly recover all the temporal frames from the k-t space data. The joint approach enables the deconvolution of the spectra using the line shape estimates from water reference data, thus compensating for field inhomogeneity induced line broadening artifacts. This spectral deconvolution strategy is similar in concept to the ones used in the spatial compartment modeling schemes (12, 13). We will not resort to compartment models to minimize bias. Sparse spectral regularization is used to minimize the noise amplification associated with un-regularized deconvolution.

A spiral sequence is used to acquired the MRSI data with a matrix size of $60 \times 60 \times 256$. The k-space center is heavily oversampled compared to outer k-space to minimize the SNR loss associated with extended k-space coverage. A dual resolution strategy is used to minimize the

tradeoff in recovering the signal challenged metabolites and SNR-rich nuisance signals at the same spatial resolution. Specifically, the nuisance signals are recovered at the highest possible spatial resolution to minimize the spectral leakage artifacts. By contrast, the point spread functions of the metabolites are optimized to yield acceptable SNR.

The proposed algorithm is posed as a convex optimization problem, where the criterion is the linear combination of a data consistency term, spatial smoothness penalty, and sparsity penalty. The optimal regularization parameters are chosen using L-surface method (14). We rely on an iterative reweighted algorithm to solve the criterion. The water reference priors that the algorithm relies on are (i) extracranial lipid and brain boundaries, (ii) magnetic field inhomogeneity induced line shape distortions, and (iii) coil sensitivity maps (see Fig. 1.a). We compare the proposed model based reconstruction scheme with (a) Tikhonov regularized reconstruction of the spiral data, and (b) spectra obtained using the product CSI scheme. The comparisons with CSI data demonstrate the ability of the proposed scheme to provide comparable spectral quality, despite the significantly reduced scan time and improved spatial resolution. The comparisons with Tikhonov reconstructions demonstrates the utility of the deconvolution scheme in minimizing line shape distortions and noise. This work further improves upon (15), where the recovery of MRSI data from single channel EPSI acquisition was considered. The generalization of the algorithm in (15) to the recovery of non-Cartesian multichannel data enables us to exploit the improved SNR efficiency of variable density spiral sequences to improve the spatial resolution, thereby further reducing spectral leakage and line shape distortions. In addition, we have further improved and simplified the spectral model by exploiting the spatial-spectral properties of the data.

METHODS

We propose to minimize field inhomogeneity induced spectral distortions using a sparse spectral deconvolution algorithm. A dual resolution reconstruction strategy, where nuisance signals are recovered at the highest possible spatial resolution, while the spatial point spread functions of the metabolites are optimized to yield acceptable SNR, is used. The proposed reconstruction algorithm rely on the following spatial and spectral priors that are estimated from the water reference data (see Fig. 1.a):

1. the line shape distortion function $\alpha[\mathbf{r}]$,

2. the coil sensitivity estimates $s_i[\mathbf{r}]$, and

3. spatial spectral supports of the metabolite Ω_m and nuisance signals $\Omega_{\rm n}$ (see Fig. 1.b).

Acquisition Scheme

A spin echo spiral MRSI sequence was implemented on Siemens 3T Tim Trio scanner to acquire MRSI data with a matrix size of 60x60x256. The trajectory was computed using the expressions in (16) with twenty-four spatial interleaves. The details of the trajectory and its plots are provided in Fig.1.(c)-(d). The chemical shift dimension is encoded by repeatedly playing out spiral gradients, sandwiched between flyback gradients. The duration of each spiral echo (echospace) is 1.68 ms, resulting in a spectral bandwidth of 595 Hz (4.8 ppm). A slew rate of 80 T/m/s and a maximum gradient amplitude of 22.4 mT/m were assumed. With a field of view of 240mm $\times$ 240mm and a matrix size of 60×60, the maximum achievable in-plane spatial resolution is 4×4 mm^2. The reconstruction algorithm recovers the nuisance signals at this resolution, while the nominal voxel sizes of the metabolite region are approximately 6×6 mm^2 in the five average case and around 8×8 mm^2 in the three average case. The spectral resolution is 2.32 Hz. The heavy oversampling at the center, offered by the spiral trajectory (≈8 fold), ensures that most of the scan time is devoted to acquiring the lower k-space samples (3, 11), thus providing better SNR/scan time compared to a Cartesian scheme with similar resolution. Six to eight fat saturation bands were used to suppress extra-cranial lipids. The first repetition of the sequence is used to acquire water reference data.

System Model

The spatial spectral MRSI signal, denoted by $\rho(\mathbf{x}, f)$, is assumed to be zero outside the spatial-spectral region corresponding to the head, indicated by $\Omega = \Omega_m \bigcup \Omega_n$. This includes all pixels within the head region and all chemical shift frequencies (see Fig. 1.b). The spectral support of the metabolites are fixed as shown in Fig. 1; it includes the entire range of chemical shifts, excluding a 100 Hz band around the water frequency. The spatial supports are estimated from water and fat images, obtained by spectral integration of water reference data in a 1 ppm range. These images are thresholded to obtain the head and fat regions. A two pixel border around the head is added to the fat region to minimize the risk of fat leakage.

The measured MRSI signal from the i^{th} coil is modeled as

$$m_i\left[\mathbf{k},t\right]=\sum_{(\mathbf{r},f)\in\Omega} s_i(\mathbf{r})\rho(\mathbf{r},f)\qquad \underbrace{\exp^{-\alpha[\mathbf{r}]t}}_{\text{lineshape distortion}}\qquad \underbrace{\exp^{-j\left(2\pi\mathbf{k}^T\mathbf{r}-ft\right)}}_{\text{k-space encoding}} \tag{1}$$

Here, $\mathbf{r}$ denotes the spatial location and f is the chemical shift frequency. $s_i[\mathbf{r}]$ is the sensitivity of the i^{th} coil. Here,

$$\alpha[\mathbf{r}]=j\triangle\omega_0[\mathbf{r}]+\frac{1}{T_2^*[\mathbf{r}]}, \tag{2}$$

where $\triangle\omega_0=\gamma\triangle B_0$ is the field inhomogeneity induced frequency shift, while the decay term $\frac{1}{T_2^*}$ captures the intra-voxel dephasing effects. The linear measurement model [1] is compactly expressed as $\mathbf{m}=\boldsymbol{\mathcal{A}}(\boldsymbol{\rho})$, where $\boldsymbol{\mathcal{A}}$ is termed as the system model.

Reconstruction Algorithm

The dual resolution spectral deconvolution algorithm to recover the MRSI data is formulated as the optimization problem:

$$\rho^*[\mathbf{r},f]=\arg\min_{\rho}\ \underbrace{\|\boldsymbol{\mathcal{A}}(\boldsymbol{\rho})-\mathbf{m}\|^2}_{\text{data consistency}}+\underbrace{\lambda_1\sum_{(\mathbf{r},f)\in\Omega_{\text{m}}}|\triangle\boldsymbol{\rho}(\mathbf{r},f)|^2}_{\text{spatial regularization}}+\underbrace{\lambda_2\sum_{(\mathbf{r},f)\in\Omega_{\text{m}}}|\boldsymbol{\rho}(\mathbf{r},f)|}_{\text{spectral regularization}} \tag{3}$$

The first term in [3] is the data-consistency term, while the second term is the Tikhonov smoothness penalty of ρ restricted to the brain region Ω_{m}. Here, $\triangle\boldsymbol{\rho}$ are the spatial finite differences of $\boldsymbol{\rho}$, specified by:

$$\triangle\boldsymbol{\rho}=\begin{cases}(\partial_x\rho,\partial_y\rho) & \text{if}\quad \mathbf{r}\in\Omega_{\text{m}}\\ \mathbf{0} & \text{else}\quad .\end{cases} \tag{4}$$

Here, $\partial_x\boldsymbol{\rho}=\boldsymbol{\rho}(\mathbf{r}+[1,0],f)-\boldsymbol{\rho}(\mathbf{r},f)$ and $\partial_y\boldsymbol{\rho}=\boldsymbol{\rho}(\mathbf{r}+[0,1],f)-\boldsymbol{\rho}(\mathbf{r},f)$. The restriction of the spatial regularization to the metabolite region guarantees the narrowest possible point spread function for the fat and water signals, thus minimizing the risk of spectral leakage. By contrast, the point-spread functions in the brain region are optimized to ensure robust metabolite estimates.

Since the line-shape distortions are incorporated in the system model $\boldsymbol{\mathcal{A}}$, the optimization problem [3] involves the deconvolution of these distortions. The spectral regularization penalty is used to minimize the noise amplification associated with deconvolution. This penalty is also restricted to Ω_{m} to minimize leakage from nuisance signals. We solve [3] using an iterative reweighting algorithm, described in detail in (15). Our current MATLAB implementation of the algorithm takes roughly fifteen minutes/slice on a quad core linux machine with NVDIA Tesla graphical processing

unit. We use spatial regularization for all the reconstructions (including Tikhonov reconstructions), while spectral regularization is only used with the proposed method. We determine the optimal parameters using the L-surface method (14).

Experiments and comparisons

The proposed scheme is compared against **(a)** Tikhonov regularized reconstruction, which does not use line shape priors and spectral regularization, and **(b)** spectra obtained using the product CSI scheme on a spectroscopy phantom and human brain. Experimental data was acquired from five normal human subjects on Siemens Trio 3T scanners at University of Rochester (UR) and University of Iowa (UI). The results from two of these scans are shown in the paper. The studies were approved by the research subjects review boards at both institutions and informed consents were obtained. The 12 channel head array was used with a field of view of 240x240 mm^2. The first scan (TR=2s, TE=40ms, #averages=5, slice thickness=10mm,#slices=2) is used to compare against Tikhonov reconstruction. The total scan time for this acquisition was 9.6 minutes (4.8 minutes/slice), including the acquisition of the water reference data. Similar parameters were used in the comparison against CSI (except TR=1.5s); the total scan time for this acquisition was 7.2 minutes (3.6 minutes/slice).

Since the Tikhonov scheme does not use any spectral regularization, it is equivalent to recovering each temporal frame independently; this approach is similar to most of the current MRSI algorithms (3–6, 11, 17). The smoothness regularization parameter in Tikhonov scheme was set using L-curve analysis as $\lambda = 3 \times 10^{-3}$. The Tikhonov reconstructed spectra were shifted to the correct locations using the field inhomogeneity estimates obtained from water reference data. The metabolite maps of N-acetyl aspartate (NAA), creatine (Cr), and choline (Cho) were recovered from the estimated spectra by integrating five spectral frames (equivalent to 11.6 Hz).

The CSI data from the GE spectroscopy phantom was acquired with 32x32 matrix, TR=1.5 seconds, TE=40ms. The entire phantom was included in the region of interest and the acquisition time was approximately 20 minutes. The *in-vivo* CSI data was acquired with a 24x24 matrix, TR=1.5 seconds, TE=40ms in approximately 10 minutes. Here, the ROI was restricted to a rectangular region within the brain. These comparisons are challenging due to the discrepancy between the two acquisition schemes. Since the CSI sequence relies on PRESS excitation, it suffers from spatial mismatch due to chemical shift (18). In addition, the spatial resolution of both schemes are drastically different. To match up the two datasets, we multiplied the recovered spiral MRSI by

a mask corresponding to the VOI derived from CSI acquisitions, followed by spatial smoothing to match the spatial resolution.

RESULTS

Selection of optimal regularization parameters

The L-surface analysis yielded the optimal regularization parameters $\lambda_1 = 2 \times 10^{-4}$; $\lambda_2 = 1 \times 10^{-5}$ for the dataset with five signal averages. Since it is difficult to display the entire L-surface, we show the corresponding L-curves in Fig. 2.a. These curves are generated by varying one parameter, while setting the other one to the optimal value obtained from the L-surface analysis. The Choline maps and the spectra for different parameter choices are shown. We observe that the optimal λ_1 provides a good compromise between over-smoothing and noise suppression, while the selection of λ_2 gives a good tradeoff between suppression of small spectral details and noise suppression. We observe that the parameters does not change considerably from scan to scan. The second dataset that was also acquired with five averages is reconstructed using the above parameters. We repeated the L-surface analysis for three and one averages, respectively. The optimal parameters in both of these cases were $\lambda_1 = 4 \times 10^{-4}$; $\lambda_2 = 1 \times 10^{-5}$. The higher spatial regularization (λ_1) compared to five average setting results in larger voxel dimensions (see below); more spatial smoothing is required to obtain reliable data when the measurements are more noisy.

To further characterize the reconstructions, we consider the recovery of a numerical phantom from its measurements in Fig. 2. (b)-(e). The numerical phantom have point spectra on two different spectral frames (100 and 110), at locations specified by the dots in Fig. 2.(b) and Fig. 2.(e). The 100th frame of the recovered data set with the proposed algorithm using the optimal parameters and Tikhonov scheme are shown in (d) and (e). We observe that the point spectra in the lipid region are recovered exactly since no regularization is applied in this region. In contrast, the point objects are recovered as broad blobs in the metabolite regions due to spatial regularization. The full width at half maximum of these blobs was observed to be approximately 1.5 pixels (6 mm). The spectral deconvolution scheme is capable of minimizing the cross talk in the spectra (see residual signal from 110th frame in Tikhonov scheme).

Comparison with Tikhonov regularized reconstructions

The comparison of the proposed reconstruction scheme with Tikhonov regularized least square algorithm on spiral MRSI data is shown in Fig.3. Since the proposed scheme uses the line shape priors to deconvolve the spectra, it is capable of reducing field inhomogeneity induced intra-voxel line broadening. The improvement in lineshapes also translates to improved metabolite maps (see top rows of Fig.3). The improvement is more pronounced with metabolites with comparatively smaller peaks (Choline); the vulnerablity to noise and baseline fluctuations increases with decreased peak heights. The proposed algorithm only relies on the masks of the brain regions and line shapes from the water reference data. Hence, the image contrast in the reconstructions are entirely from the measured MRSI data.

The robustness of the algorithms to noise is studied by recovering the MRSI data from three and one averages, respectively. The results are shown in Fig. 4. The scan times per slice for three and one average, along with the water reference dataset, are 3.2 minutes and 1.6 minutes, respectively. It is seen that the spectra obtained using the proposed scheme with three averages are more-or-less comparable to the case with five averages. Since λ_1 is set to $4e^{-4}$, the full width at half maximum of the spatial point spread functions in this case is approximately 2 pixels (8 mm). Thus the price to pay for reduced scan time is decreased spatial resolution.

Comparison with CSI data

The comparison of the proposed scheme with CSI data are shown in Fig. 5. We used the same shim setting for both the scans to make the two experiments comparable.The spectra obtained by both schemes are comparable in most regions of the phantom; the CSI spectra are corrupted by spectral leakage and lineshape distortions in the bottom regions, while the proposed scheme is able to recover reliable spectra, thanks to higher k-space coverage, dual resolution reconstruction strategy, and spectral deconvolution. In the in-vivo experiment, the optimization of the shim setting to the CSI acquisition resulted in large field inhomogeneity in other brain regions (e.g. top of the ROI in Fig. 5.d-f), resulting in line-shape distortions. We observe that the amplitudes do not match up due to chemical shifts as well as differences in excitation profiles. However, significant similarities between the spectral shapes obtained by both schemes can be observed.

DISCUSSION

The proposed iterative reconstruction algorithm relies on line shape priors, spatial-spectral information about the metabolite and extra-cranial fat regions, and spectral sparsity, to minimize line shape distortions. Since the proposed scheme uses a dual resolution strategy, it can reduce spectral leakage without compromising the SNR of the metabolites. While the proposed scheme uses the same priors as the MIDAS framework (19), there are fundamental differences. MIDAS is designed for Cartesian acquisitions; its extension of this framework to non-Cartesian acquisitions is not straightforward. Additionally, the proposed iterative algorithm can account for the priors during the reconstruction process rather than post-reconstruction, asx in (19). The comparisons of the proposed scheme using in vivo data shows that the proposed reconstruction scheme can reduce field inhomogeneity induced spectral distortions, and spectral leakage, when compared with Tikhonov reconstruction. The reduction of distortions due to extended k-space coverage more than compensate for the associated SNR loss, which is consistent with the observation in (20). In comparison to (20), we further minimize the SNR loss using variable density trajectories and extended the k-space coverage.

ACKNOWLEDGEMENTS

We thank the anonymous reviewers, whose comments have considerably improved the quality of the manuscript. This study was supported by NSF grants CCF-0844812, CCF-1116067, and American Cancer Society grant RSG CCE-121672.

References

[1] AA Maudsley, C. Domenig, V. Govind, A. Darkazanli, C. Studholme, K. Arheart, and C. Bloomer. Mapping of brain metabolite distributions by volumetric proton mr spectroscopic imaging (mrsi). *Magnetic Resonance in Medicine*, 61(3):548–559, 2009.

[2] R. Otazo, B. Mueller, K. Ugurbil, L. Wald, and S. Posse. Signal-to-noise ratio and spectral linewidth improvements between 1.5 and 7 tesla in proton echo-planar spectroscopic imaging. *Magnetic resonance in medicine*, 56(6):1200–1210, 2006.

[3] E. Adalsteinsson, J. Star-Lack, C.H. Meyer, and D.M. Spielman. Reduced spatial side lobes in chemical-shift imaging. *Magnetic resonance in medicine*, 42(2):314–323, 1999.

[4] C. Liu, R. Bammer, and M.E. Moseley. Parallel imaging reconstruction for arbitrary trajectories using k-space sparse matrices (kspa). *Magnetic Resonance in Medicine*, 58(6):1171–1181, 2007.

[5] D. Mayer, D.H. Kim, D.M. Spielman, and R. Bammer. Fast parallel spiral chemical shift imaging at 3t using iterative sense reconstruction. *Magnetic Resonance in Medicine*, 59(4):891–897, 2008.

[6] S. Posse, R. Otazo, S.Y. Tsai, A.E. Yoshimoto, and F.H. Lin. Single-shot magnetic resonance spectroscopic imaging with partial parallel imaging. *Magnetic Resonance in Medicine*, 61(3): 541–547, 2009.

[7] X. Hu, D.N. Levin, P.C. Lauterbur, and T. Spraggins. Slim: Spectral localization by imaging. *Magnetic resonance in medicine*, 8(3):314–322, 1988.

[8] Z.P. Liang and PC Lauterbur. A generalized series approach to mr spectroscopic imaging. *Medical Imaging, IEEE Transactions on*, 10(2):132–137, 1991.

[9] J. Kornak, K. Young, B.J. Soher, and A.A. Maudsley. Bayesian k-space–time reconstruction of mr spectroscopic imaging for enhanced resolution. *Medical Imaging, IEEE Transactions on*, 29(7):1333–1350, 2010.

[10] Y. Bao and A.A. Maudsley. Improved reconstruction for mr spectroscopic imaging. *Medical Imaging, IEEE Transactions on*, 26(5):686–695, 2007.

[11] E. Adalsteinsson, P. Irarrazabal, S. Topp, C. Meyer, A. Macovski, and D.M. Spielman. Volumetric spectroscopic imaging with spiral-based k-space trajectories. *Magnetic resonance in medicine*, 39(6):889–898, 1998.

[12] I. Khalidov, D. Van De Ville, M. Jacob, F. Lazeyras, M. Unser, et al. Bslim: Spectral localization by imaging with explicit b0 field inhomogeneity compensation. *IEEE transactions on medical imaging*, 26(7):990, 2007.

[13] M. Jacob, X. Zhu, A. Ebel, N. Schuff, and Z.P. Liang. Improved model-based magnetic resonance spectroscopic imaging. *Medical Imaging, IEEE Transactions on*, 26(10):1305–1318, 2007.

[14] M. Belge, M.E. Kilmer, and E.L. Miller. Efficient determination of multiple regularization parameters in a generalized l-curve framework. *Inverse Problems*, 18(4):1161, 2002.

[15] R. Eslami and M. Jacob. Robust reconstruction of mrsi data using a sparse spectral model and high resolution mri priors. *Medical Imaging, IEEE Transactions on*, 29(6):1297–1309, 2010.

[16] G.H. Glover et al. Simple analytic spiral k-space algorithm. *Magnetic Resonance in medicine*, 42(2):412–415, 1999.

[17] S.Y. Tsai, R. Otazo, S. Posse, Y.R. Lin, H.W. Chung, L.L. Wald, G.C. Wiggins, and F.H. Lin. Accelerated proton echo planar spectroscopic imaging (pepsi) using grappa with a 32-channel phased-array coil. *Magnetic Resonance in Medicine*, 59(5):989–998, 2008.

[18] T.K.C. Tran, D.B. Vigneron, N. Sailasuta, J. Tropp, P. Le Roux, J. Kurhanewicz, S. Nelson, and R. Hurd. Very selective suppression pulses for clinical mrsi studies of brain and prostate cancer. *Magnetic resonance in medicine*, 43(1):23–33, 2000.

[19] AA Maudsley, A. Darkazanli, JR Alger, LO Hall, N. Schuff, C. Studholme, Y. Yu, A. Ebel, A. Frew, D. Goldgof, et al. Comprehensive processing, display and analysis for in vivo mr spectroscopic imaging. *NMR in Biomedicine*, 19(4):492–503, 2006.

[20] A. Ebel and A.A. Maudsley. Improved spectral quality for 3d mr spectroscopic imaging using a high spatial resolution acquisition strategy. *Magnetic resonance imaging*, 21(2):113–120, 2003.

Figure Legends

Figure 1: Main aspects of the proposed scheme. (a) Illustration of the data-processing pipeline. The reconstruction algorithm relies on (i) line-shapes, (ii) spatial-spectral supports, and (iii) coil sensitivity functions, which are estimated from water reference data. (b) spatial spectral supports of the metabolite (Ω_m) and nuisance signals (Ω_n), which are shown in gray and white colors, respectively. Specifically, the slice of the support function corresponding to the NAA frequency is shown on left, while the x-f plot along the red line shown in the right. The regularization terms are only applied to Ω_m, while the signal is restricted to $\Omega = \Omega_{\rm m} \bigcup \Omega_{\rm n}$. The spiral trajectory is illustrated in (c) and (d); we plot $k_x.F$ vs $k_y.F$, where F is the field of view. The chemical shift dimension is encoded by repeatedly playing out spiral gradients, sandwiched between flyback gradients. Four of the 24 spatial interleaves are shown in different colors.

Figure 2: Choice of regularization parameters: We determine the optimal regularization parameters ($\lambda_1 = 2e^{-4}; \lambda_2 = 1e^{-5}$) using the L-surface approach (14). We plot the L-curve by setting $\lambda_2 = 1e^{-5}$ in the top-left figure; we change λ_1 and plot the data consistency error against the smoothness penalty. The corresponding Choline images are also shown. Similarly, the L-curve corresponding to $\lambda_1 = 2e^{-4}$, is shown in top right. Note that the data consistency error is only 1.2% of the variance of the measured data, which confirms that the regularization is moderate and does not over smooth/bias the reconstructions. In the bottom row, we consider the recovery of a numerical phantom from it sensitivity weighted spiral data, generated using the model in [1]. The anatomy and line shape priors are assumed from slice 2 of the dataset in Fig. 4. The numerical phantom has point spectra, in frames 100 and 110, shown on points indicated in (b) and (c) . The signal intensity is zero at all other points. The signal was recovered using the proposed scheme with optimal parameters and standard Tikhonov regularization ($\lambda_1 = 3e-3; \lambda_2 = 0$). The peak integral plots of the reconstructions are shown.

Figure 3: Comparison of the proposed reconstructions with Tikhonov regularized reconstructions. The two columns corresponds to data from from first and second slices, respectively. The metabolite maps are shown in the first row. The spectra at points indicated by the red dots on the water image and spatial masks (in the fourth row) are shown in the second and third rows, respectively. The line shapes estimated from the water reference data is shown in the bottom row.

Figure 4: Robustness of the algorithm to measurement noise. We study the performance of the algorithm when the number of averages are low. The optimal regularization parameters were determined using the L surface method to be $\lambda_1 = 4e^{-4}$ and $\lambda_2 = 1e^{-5}$ in both cases. The equivalent acquisition times are 3.2 minutes/slice and 1.6 minutes/slice, respectively, including the time to acquire the water reference data.

Figure 5: Comparison of the proposed scheme with chemical shift imaging. The top row corresponds to the data acquired from a GE spectroscopic phantom, while the bottom row is acquired from a human volunteer. The PRESS box spanned the entire phantom, while it was restricted to a rectangular window in the *in-vivo* experiment. We added a vitamin E pill at the bottom for localization in the phantom experiment, which was outside of the PRESS box (see blob in the image). The NAA maps estimated by the proposed scheme, after smoothing to match the resolution with CSI data, is shown in (c)&(f), respectively. The spectra at the points indicated by the dots are shown in (a)&(d) and (b)&(e), respectively. It is seen that the bottom row of the CSI data (32x32 matrix) is corrupted by spectral leakage and field map distortions, even though the PRESS box excluded the pill. The proposed scheme is able to recover reliable spectra in these regions, thanks to the better k-space coverage, the dual resolution reconstruction strategy, and spectral deconvolution. As explained in the text, the *in-vivo* comparisons are challenging due to a variety of technical reasons. The SNR and line widths of the proposed spectra resemble the CSI spectra in the bottom regions of the PRESS box; the top regions are corrupted by large field inhomogeneity variations due to shim settings (see text).

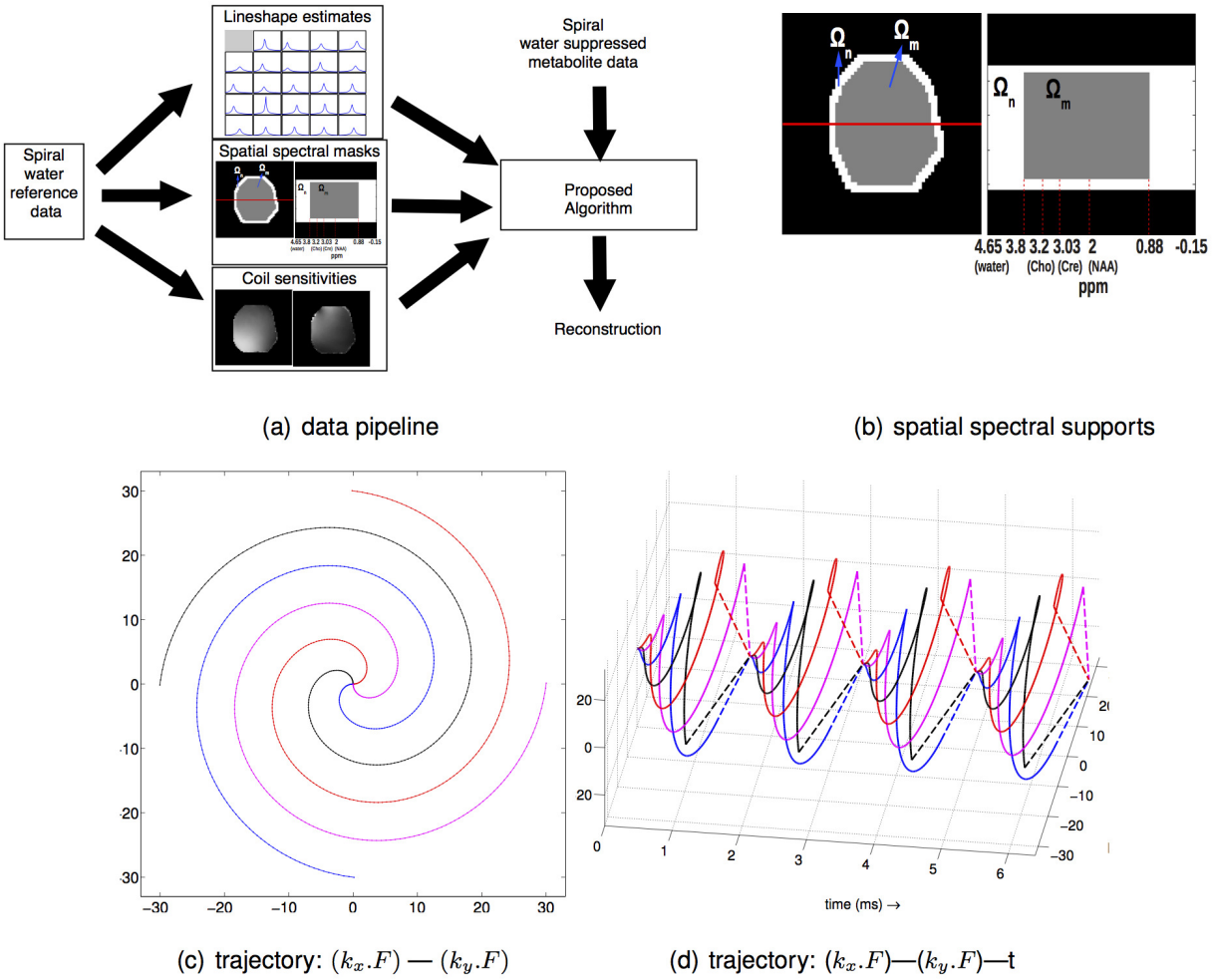

(a) data pipeline

(b) spatial spectral supports

(c) trajectory: $(k_x.F)$ — $(k_y.F)$

(d) trajectory: $(k_x.F)$—$(k_y.F)$—t

Figure 1: Main aspects of the proposed scheme. (a) Illustration of the data-processing pipeline. The reconstruction algorithm relies on (i) line-shapes, (ii) spatial-spectral supports, and (iii) coil sensitivity functions, which are estimated from water reference data. (b) spatial spectral supports of the metabolite (Ω_m) and nuisance signals (Ω_n), which are shown in gray and white colors, respectively. Specifically, the slice of the support function corresponding to the NAA frequency is shown on left, while the x-f plot along the red line shown in the right. The regularization terms are only applied to Ω_m, while the signal is restricted to $\Omega = \Omega_{\mathrm{m}} \bigcup \Omega_{\mathrm{n}}$. The spiral trajectory is illustrated in (c) and (d); we plot $k_x.F$ vs $k_y.F$, where F is the field of view. The chemical shift dimension is encoded by repeatedly playing out spiral gradients, sandwiched between flyback gradients. Four of the 24 spatial interleaves are shown in different colors.

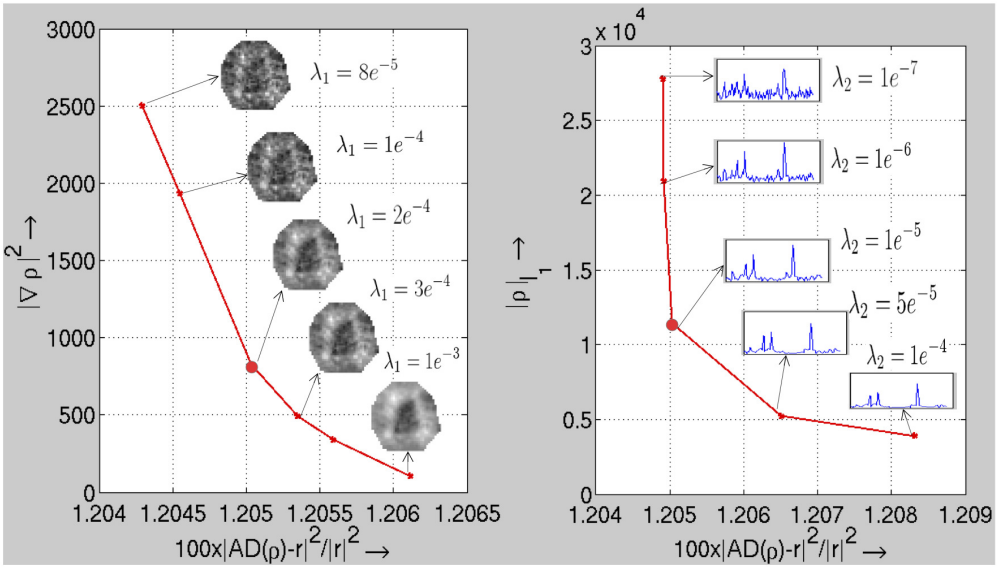

(a) Choice of regularization parameters

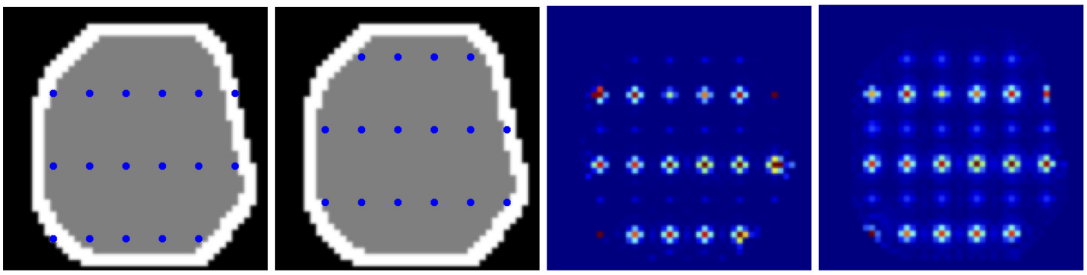

(b) Peaks at frame 100 (c) Peaks at frame 110 (d) Proposed: 100th frame (e) Tikhonov: 100th frame

Figure 2: Choice of regularization parameters: We determine the optimal regularization parameters ($\lambda_1 = 2e^{-4}; \lambda_2 = 1e^{-5}$) using the L-surface approach (14). We plot the L-curve by setting $\lambda_2 = 1e^{-5}$ in the top-left figure; we change λ_1 and plot the data consistency error against the smoothness penalty. The corresponding Choline images are also shown. Similarly, the L-curve corresponding to $\lambda_1 = 2e^{-4}$, is shown in top right. Note that the data consistency error is only 1.2% of the variance of the measured data, which confirms that the regularization is moderate and does not over smooth/bias the reconstructions. In the bottom row, we consider the recovery of a numerical phantom from it sensitivity weighted spiral data, generated using the model in [1]. The anatomy and line shape priors are assumed from slice 2 of the dataset in Fig. 4. The numerical phantom has point spectra, in frames 100 and 110, shown on points indicated in (b) and (c) . The signal intensity is zero at all other points. The signal was recovered using the proposed scheme with optimal parameters and standard Tikhonov regularization ($\lambda_1 = 3e-3; \lambda_2 = 0$). The peak integral plots of the reconstructions are shown.

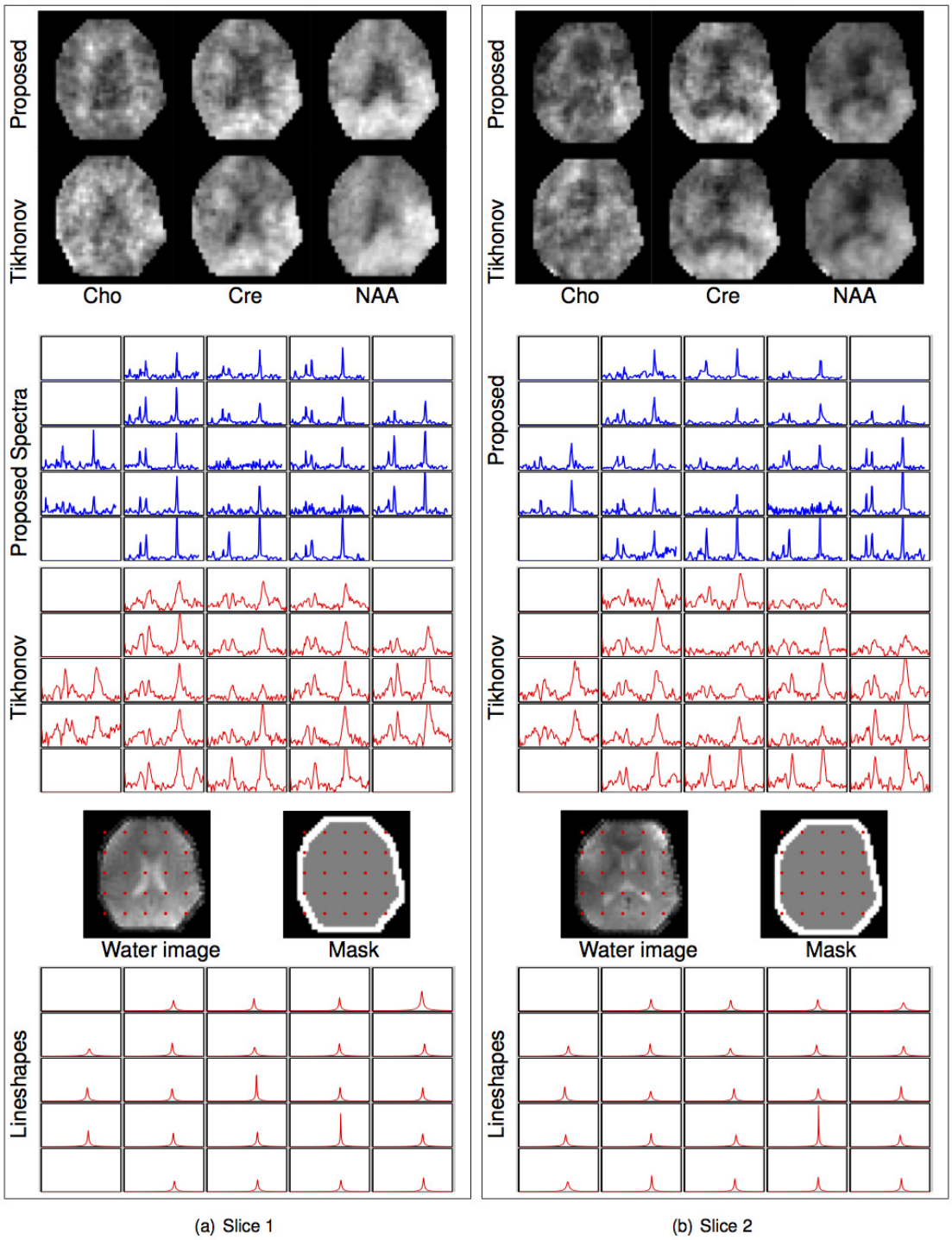

Figure 3: Comparison of the proposed reconstructions with Tikhonov regularized reconstructions. The two columns corresponds to data from from first and second slices, respectively. The metabolite maps are shown in the first row. The spectra at points indicated by the red dots on the water image and spatial masks (in the fourth row) are shown in the second and third rows, respectively. The line shapes estimated from the water reference data is shown in the bottom row.

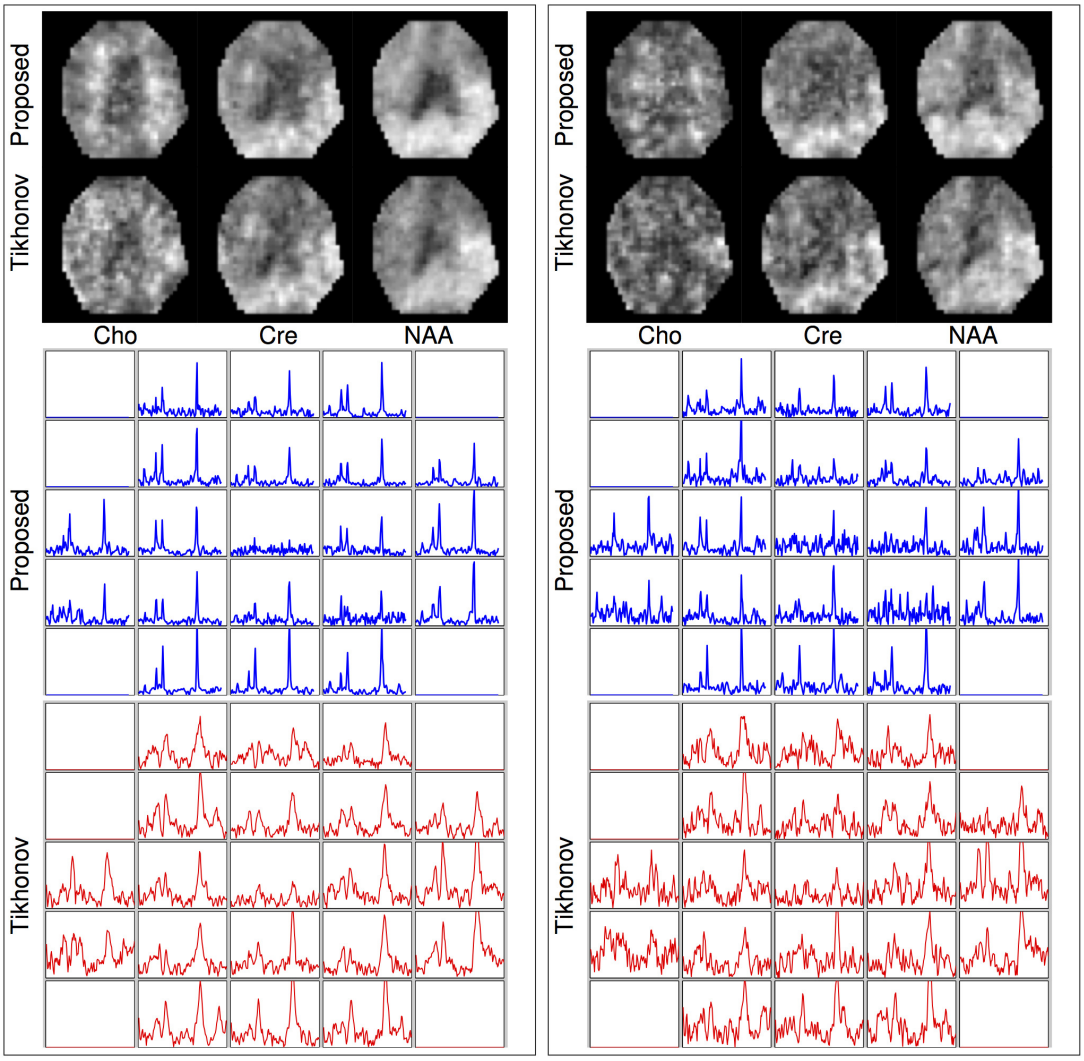

(a) 3 averages;2.4 mins/slice

(b) 1 average; 48 seconds/slice

Figure 4: Robustness of the algorithm to measurement noise. We study the performance of the algorithm when the number of averages are low. The optimal regularization parameters were determined using the L surface method to be $\lambda_1 = 4e^{-4}$ and $\lambda_2 = 1e^{-5}$ in both cases. The equivalent acquisition times are 3.2 minutes/slice and 1.6 minutes/slice, respectively, including the time to acquire the water reference data.

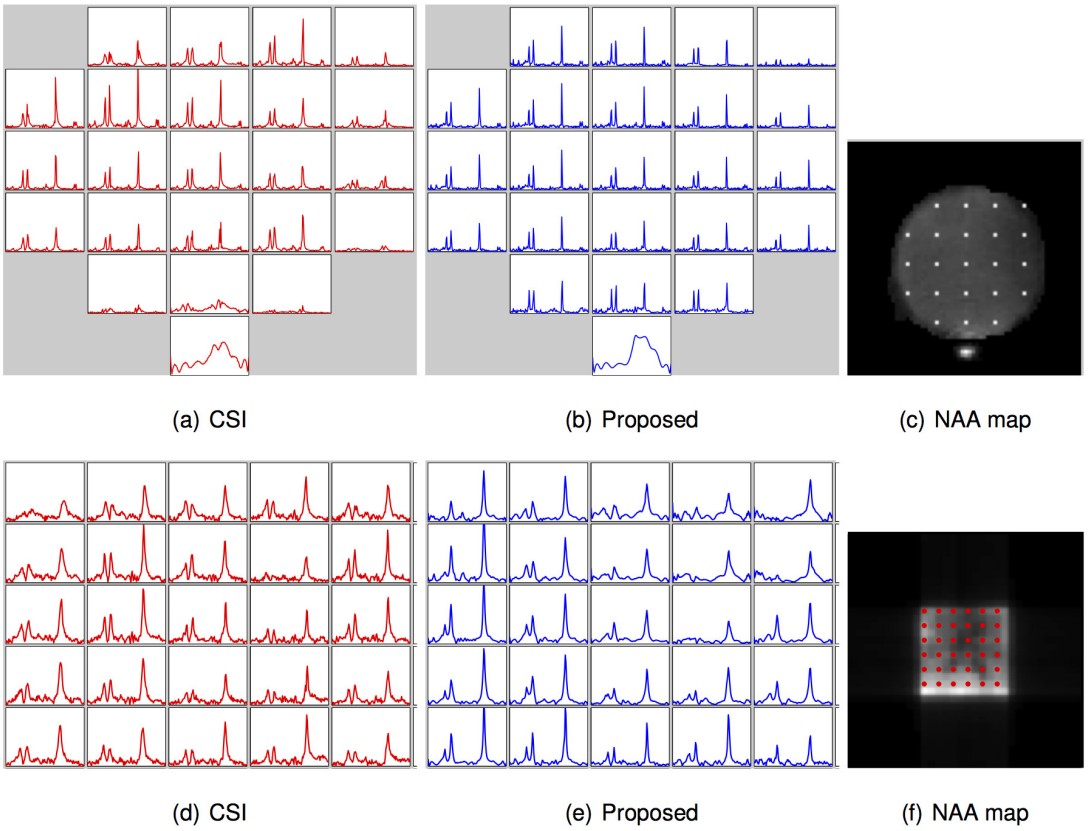

Figure 5: Comparison of the proposed scheme with chemical shift imaging. The top row corresponds to the data acquired from a GE spectroscopic phantom, while the bottom row is acquired from a human volunteer. The PRESS box spanned the entire phantom, while it was restricted to a rectangular window in the *in-vivo* experiment. We added a vitamin E pill at the bottom for localization in the phantom experiment, which was outside of the PRESS box (see blob in the image). The NAA maps estimated by the proposed scheme, after smoothing to match the resolution with CSI data, is shown in (c)&(f), respectively. The spectra at the points indicated by the dots are shown in (a)&(d) and (b)&(e), respectively. It is seen that the bottom row of the CSI data (32x32 matrix) is corrupted by spectral leakage and field map distortions, even though the PRESS box excluded the pill. The proposed scheme is able to recover reliable spectra in these regions, thanks to the better k-space coverage, the dual resolution reconstruction strategy, and spectral deconvolution. As explained in the text, the *in-vivo* comparisons are challenging due to a variety of technical reasons. The SNR and line widths of the proposed spectra resemble the CSI spectra in the bottom regions of the PRESS box; the top regions are corrupted by large field inhomogeneity variations due to shim settings (see text).